AEROSPACE REPORT NO.
TR-0091(6470-03)-1

AD-A256 462

Frequency Shifts in a Rubidium Frequency Standard
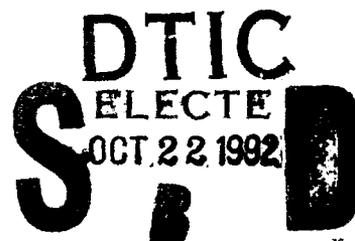# Due to Coupling to Another Standard

Prepared by

B. JADUSZLIWER, R. A. COOK, and R. P. FRUEHOLZ
Electronics Technology Center
Technology Operations

15 October 1991

DTIC
ELECTE
OCT 22 1992
S B D

Prepared for

Engineering and Technology Group

THE AEROSPACE CORPORATION
El Segundo, California

92-27670

QUANG BUI, Lt, USAF
MOIE Program Manager

CYNTHIA B. TENEROWICZ, 1Lt, USAF
Payload Development Engineer
GPS Space Segment

REPORT DOCUMENTATION PAGE

1a. REPORT SECURITY CLASSIFICATION Unclassified		1b. RESTRICTIVE MARKINGS			
2a. SECURITY CLASSIFICATION AUTHORITY		3. DISTRIBUTION/AVAILABILITY OF REPORT Approved for public release; distribution unlimited			
2b. DECLASSIFICATION/DOWNGRADING SCHEDULE					
4. PERFORMING ORGANIZATION REPORT NUMBER(S) TR-0091(6470-03)-1		5. MONITORING ORGANIZATION REPORT NUMBER(S) SMC-TR-92-48			
6a. NAME OF PERFORMING ORGANIZATION The Aerospace Corporation Technology Operations	6b. OFFICE SYMBOL (If applicable)	7a. NAME OF MONITORING ORGANIZATION Space and Missile Systems Center			
6c. ADDRESS (City, State, and ZIP Code) El Segundo, CA 90245-4691		7b. ADDRESS (City, State, and ZIP Code) Los Angeles Air Force Base Los Angeles, CA 90009-2960			
8a. NAME OF FUNDING/SPONSORING ORGANIZATION	8b. OFFICE SYMBOL (If applicable)	9. PROCUREMENT INSTRUMENT IDENTIFICATION NUMBER F04701-88-C-0089			
8c. ADDRESS (City, State, and ZIP Code)		10. SOURCE OF FUNDING NUMBERS			
		PROGRAM ELEMENT NO.	PROJECT NO.	TASK NO.	WORK UNIT ACCESSION NO.

11. TITLE (Include Security Classification)

Frequency Shifts in a Rubidium Frequency Standard Due to Coupling to Another Standard

12. PERSONAL AUTHOR(S)
Jaduszliwer, B., Cook, R. A., and Frueholz, R. P.

13a. TYPE OF REPORT	13b. TIME COVERED FROM _____ TO _____	14. DATE OF REPORT (Year, Month, Day) 1991 October 15	15. PAGE COUNT 13

16. SUPPLEMENTARY NOTATION

COSATI CODES			18. SUBJECT TERMS (Continue on reverse if necessary and identify by block number)
FIELD	GROUP	SUB-GROUP	Atomic clock Allan Variance RF coupling

19. ABSTRACT (Continue on reverse if necessary and identify by block number)

Highly reliable timing systems, such as used on board satellites, may incorporate a hot standby atomic clock besides the active one. RF couplings between them may affect the performance of the active clock. We have investigated the effect of such couplings between two rubidium atomic clocks and found that they will add an oscillatory term to the Allan Variance of the active clock, degrading its frequency stability, and that under certain circumstances they may also shift the active clock's operating frequency. We discuss these two effects in detail, and establish the level of isolation required to render them negligible.

20. DISTRIBUTION/AVAILABILITY OF ABSTRACT UNCLASSIFIED/UNLIMITED ☐ SAME AS RPT. ☐ DTIC USERS		21. ABSTRACT SECURITY CLASSIFICATION	
22a. NAME OF RESPONSIBLE INDIVIDUAL		22b. TELEPHONE (Include Area Code)	22c. OFFICE SYMBOL

CONTENTS

FIGURES

2

INTRODUCTION

In a highly reliable timing system, it may be desirable to have two atomic frequency standards operating at all times, so that if one of them malfunctions, the other one can take over the timing function without a warm-up time lag. Also, cross checks might be performed to verify performance. Since both standards could be installed close to each other, sharing power, ground, and control wiring, the possibility of RF couplings between them causing frequency shifts in the unit being used as the system's frequency reference, or impairing its frequency stability, must be addressed. As an example, the current architecture of GPS Block IIR satellites envisions two atomic frequency standards being powered simultaneously, one as the active reference clock and the other as a hot standby; under most circumstances, both would be rubidium atomic frequency standards (RAFSs). In the satellite environment, potential couplings are definitely a concern. In order to assure that the system performance will remain within acceptable bounds, the effect of these couplings must be evaluated, and the level of isolation between clocks required to keep coupling effects acceptably small must be determined.

We have conducted an experimental program to determine the magnitude and characteristics of the effects of RF coupling between two powered RAFSs by measuring frequency shifts and Allan Variances of the active clock output as a function of the power coupled in from the hot-standby clock, and the frequency offset between both clocks. The results presented and discussed in this report have been obtained with EFRATOM FRK-L RAFSs, which were available in our laboratory.

EXPERIMENTAL APPROACH

Since the type and strength of the possible couplings between clocks will depend on the details of their construction, as well as on their relative positions and orientations, wiring, etc., an evaluation of the actual effects of those possible couplings on system performance would be extremely difficult except on the final assembled hardware. The approach we have taken instead is to identify the worst possible coupling modes, measure the effects of those couplings on clock performance, and then determine the level of isolation required between clocks to insure that system requirements will be met.

Preliminary analysis and experimentation indicated that direct coupling of the output of the standby clock into the control input of the voltage-controlled quartz crystal oscillator (VCXO) of the active clock results in the highest impact on the active clock's performance. We have investigated the behavior of the active clock in this configuration, using the experimental arrangement shown in Figure 1. The output of the standby RAFS is fed, after suitable attenuation, into the active RAFS's VCXO control point; the frequency offset, Δf, between the two RAFS and the power level coupled in, P_c, can be varied. The output frequency of the active RAFS is measured using standard heterodyning techniques. An Oscilloquartz BVA VCXO is used as the frequency reference for the frequency synthesizer and counter for integration times, τ, of up to 10^3 s. Some of our results have been extended to 10^4 integration times by replacing the BVA VCXO by an FTS Model 5000 Cesium Beam Atomic Frequency Standard (CAFS). Using this setup, we can measure active RAFS frequency shifts, δf, and Allan Deviations, $\sigma_y(\tau)$, as a function of Δf and P_c.
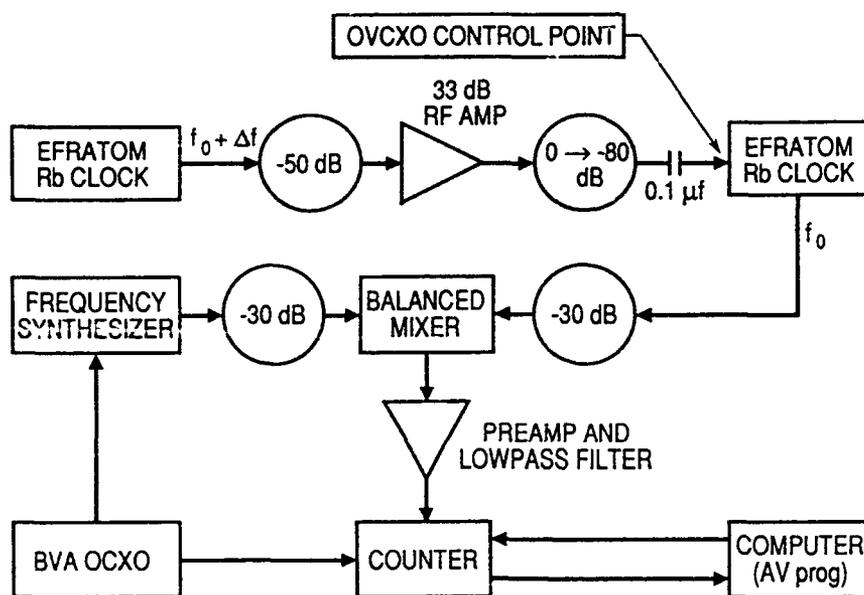
OVCXO CONTROL POINT

EFRATOM Rb CLOCK $f_0 + \Delta f$ -50 dB 33 dB RF AMP $0 \rightarrow -80$ dB 0.1 μf EFRATOM Rb CLOCK f_0

FREQUENCY SYNTHESIZER -30 dB BALANCED MIXER -30 dB

PREAMP AND LOWPASS FILTER

BVA OCXO COUNTER COMPUTER (AV prog)

Figure 1. Worst-case test configuration. The standby clock signal, offset by Δf, is injected at the VCXO voltage control pin of the active clock. A 80 dB variable attenuator allows control of the signal level. The Allan Variance and frequency shift of the active clock are measured using standard heterodyning techniques.

FREQUENCY SHIFTS

The fractional frequency shift, $\delta f/f$, of the output of the active RAFS was measured with the standby RAFS offset by $\Delta f/f \approx 10^{-9}$, 10^{-10}, and 10^{-11}. The level of the standby RAFS signal coupled at the VCXO control point was adjusted using the 0-80 dB variable attenuator shown in Figure 1. Each frequency shift measurement was corrected for drift by measuring the frequency of the uncoupled active RAFS immediately before and after it. Figure 2 presents the measured frequency shifts for the three nominal standby RAFS offsets versus the peak-to-peak coupled signal level in a log-log plot. The two short lines at the center of the plot indicate the expected slopes for a shift proportional to the coupled power (solid line) and the coupled amplitude (dashed line). Clearly, the data support a shift proportional to the power. Figure 3 shows the frequency shifts measured for each one of the three offsets versus the coupled signal power into the 50Ω termination at the VCXO control point. Each data set was fitted by a linear $\delta f/f \approx \alpha P_c$ law; the slopes are $\alpha \approx 4.9, 5.2$ and 5.5×10^{-11}/mW for $\delta f/f \approx 10^{-11}$, 10^{-10} and 10^{-9}, respectively. The differences between the coefficients are not significant, indicating that the frequency shifts are independent of the offset between the two RAFSs. The averaged frequency shift coefficient for RF power applied at the VCXO control point is $\alpha \approx 5.2 \times 10^{-11}$/mW.

The fact that the frequency shift is independent of the frequency offset between the clocks and is also present when the active clock output is fed back into its own VCXO, in which case Δf = 0, suggests some type of non-linear rectification of the coupled signal as a likely origin of the power-dependent frequency shift, with the small DC voltage thus generated coupling into the RAFS frequency control loop before the integrator.
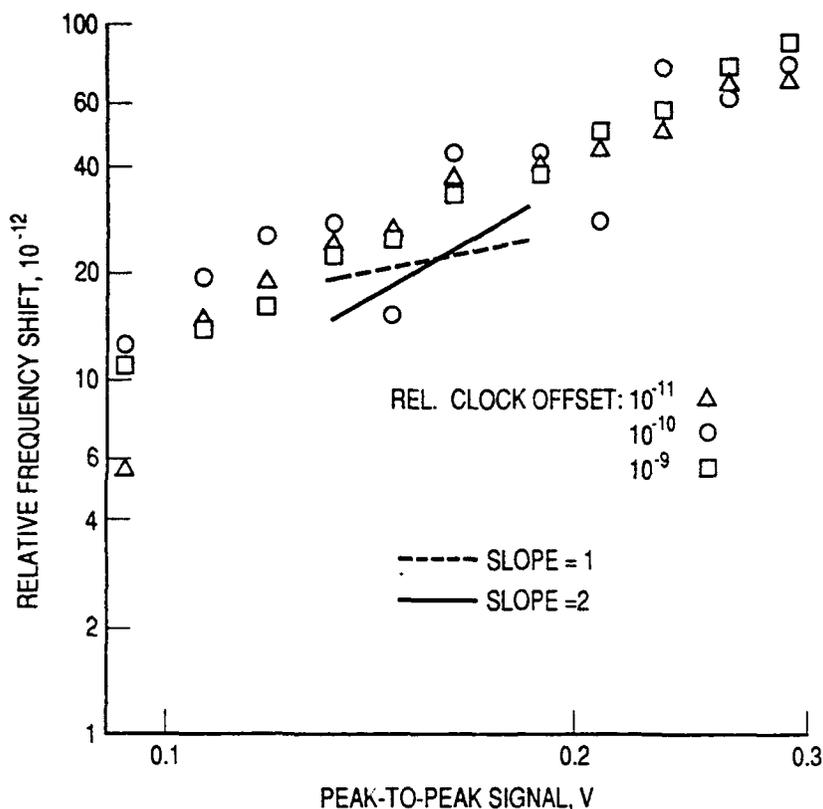
4

Figure 2. Relative frequency shift of the active clock vs. injected signal level, for three different frequency offsets between standby and active clocks, in a log-log plot. The two lines display the slopes for amplitude- or power-dependent shifts.

FREQUENCY STABILITY MEASUREMENTS

The experimental arrangement shown in Figure 1 was also used to measure the Allan Variance of the active RAFS as a function of standby RAFS offset and coupled signal level. The baseline Allan Deviation of the active RAFS was first measured with the standby RAFS unpowered and then measured again with the powered standby RAFS on the table in the same position as for all subsequent measurements, but disconnected from the active RAFS. The lack of change in $\sigma_y(\tau)$ indicates that no significant unintended couplings between the two RAFSs were present. Figures 4 and 5 show the changes induced in $\sigma_y(\tau)$ by decreasing levels of signal being coupled at the control point of the active RAFS VCXO, with the standby RAFS offset by $\Delta f/f \approx 10^{-9}$ and 10^{-10}, respectively. In each case, for high coupled power we see dramatic oscillations in the $\sigma_y(\tau)$ data, which gradually disappear as more attenuation is inserted between the two RAFSs. When the coupled power is attenuated by 50 to 70 dB, the baseline $\sigma_y(\tau)$ has largely been recovered.

The period, T, of the oscillations can be estimated from the 10 dB attenuation data to be approximately 80 s for $\Delta f/f \approx 10^{-9}$ and 540 s for $\Delta f/f \approx 10^{-10}$. It is easy to show that in each case the period is the reciprocal of the frequency offset between the clocks, corrected for the aforementioned power shift:

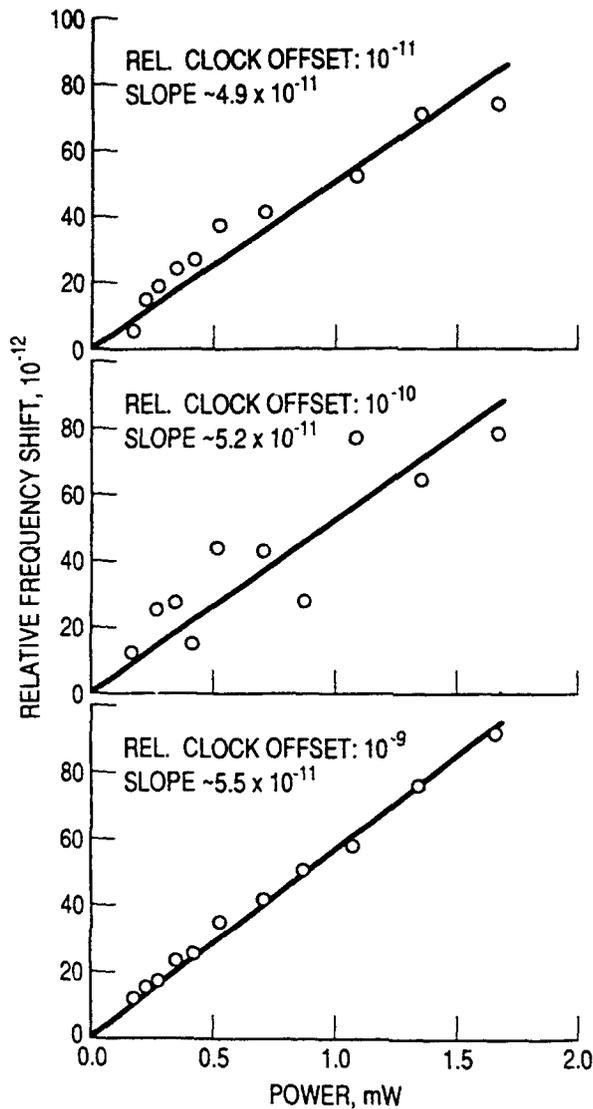$$T = \frac{1}{\Delta f + \alpha P_c f},$$

(1)

5

Figure 3. Relative frequency shift of the active clock vs. coupled power level, for three different offsets between standby and active clocks. The lines are one-parameter fits; the slopes give the coupled-power shift coefficient. The differences between the slopes are not significant.

where α is the frequency shift coefficient discussed in the preceding section. Using (1), for 10 dB attenuation, we obtain T = 75 s and T = 520 s for nominal fractional offsets 10^{-9} and 10^{-10}, respectively, in good agreement with the estimated periods. The cause of these oscillations is discussed in the last section. Longer-term $\sigma_y(\tau)$ data obtained using an FTS CAFS as the frequency reference shows that the oscillatory behavior described above also occurs for longer averaging times.

SIMULATED-SWITCH CONFIGURATION

We have also explored a second configuration, shown in Figure 6, in which the highly attenuated output of the standby clock is connected directly to the output of the active clock. This configuration simulates the situation likely to be encountered in a space vehicle, where a switch operated by telemetry

6

Figure 4. Allan Deviation of the active clock, with the standby clock offset by 1×10^{-9}, for increasing attenuator settings. With 50 dB attenuation, the measured Allan Deviation is very close to the baseline.
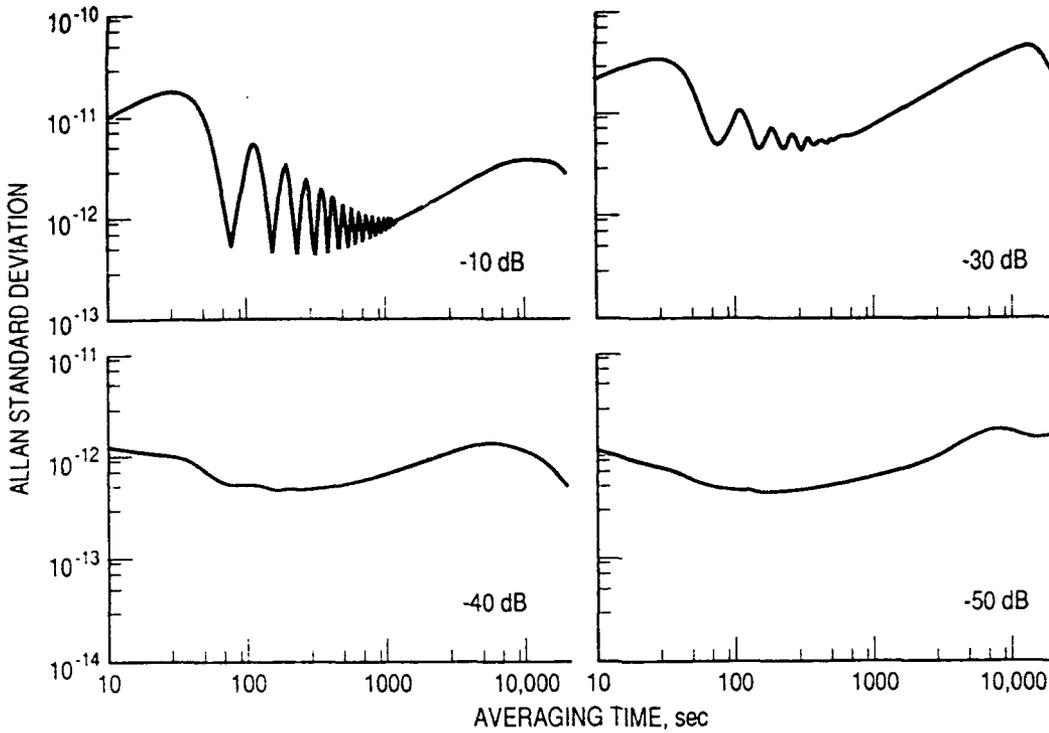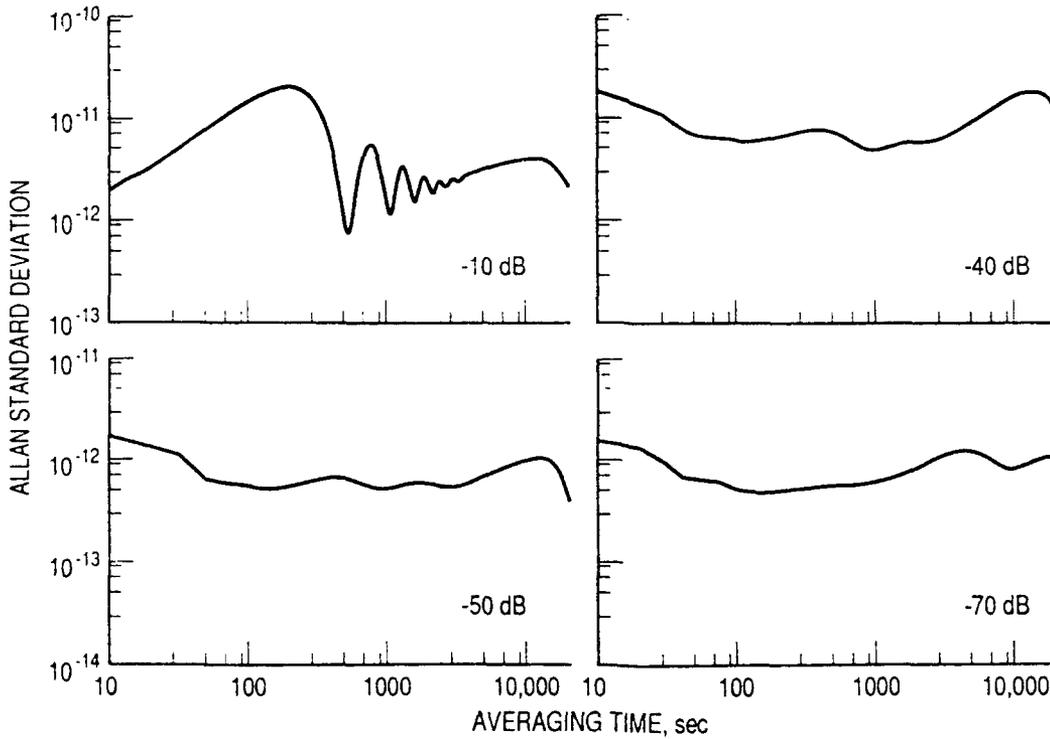

Figure 5. Allan Deviation of the active clock, with the standby clock offset by 1×10^{-10}, for increasing attenuator settings. With 70 dB of attenuation, the measured Allan Deviation is very close to baseline.
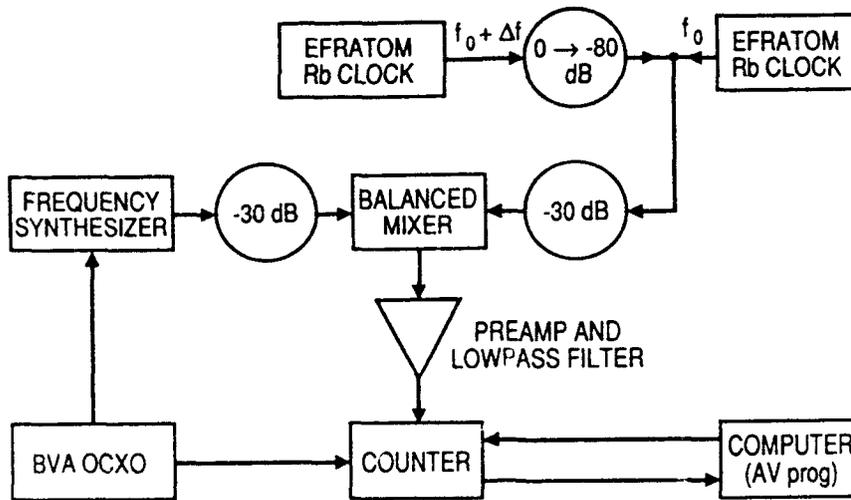
Figure 6. "Simulated switch" configuration. The output of the standby clock is
connected to the output of the active clock through an attenuator, representing
the "open" side of a switch connecting both clocks to the rest of the timing sys-
tem on board a satellite. The measuring system is the same one used for the
worst-case configuration measurements.

connects the active clock to the rest of the timing system, while inserting a large (but, for a real switch,
finite) attenuation between the standby clock and the rest of the timing system.

Measurements of the frequency of the active clock showed it to be independent of both the offset
between clocks and the signal level being coupled from the standby clock. This is understandable since
the signal coupling was done outside the active clock; thus, there is no reason to expect its frequency to
shift in any way. On the other hand, frequency stability measurements showed exactly the same type of
oscillations in the Allan Deviation as observed in the first configuration. The period was still the recip-
rocal of the frequency offset between clocks, but in this case Δf did not need to be corrected for the
coupled-power frequency shift.

In order to determine whether these oscillations involved any interaction of both signals within
the active clock, we inserted a unit-gain buffer amplifier between the active clock output and the con-
nection point. This insertion transmitted forward the signal from the active clock without change, but
added at least 33 dB of attenuation to any back- coupling of the signal of the standby clock into the
active clock via its output connector. Since the oscillations in the Allan Deviation were not affected by
this insertion, we must conclude that those oscillations simply reflect the presence in the clock signal of
an admixture of a second coherent signal at a slightly different frequency, as discussed in the next
section.

EFFECT OF A "BRIGHT LINE" OF FREQUENCY FLUCTUATIONS

The relationship between a signal's Allan Variance, $\sigma_y^2(\tau)$ and its one-sided spectral density of fre-
quency fluctuations, $S_y(f)$, is given [1] by:

$$\sigma_y^2 = 2 \int_0^\infty S_y(f) \frac{\sin^4(\pi f \tau)}{(\pi f \tau)^2} \, df .$$

(2)

8

For the situation described in the previous section, where the clock signal contains an admixture of a second coherent signal, offset by Δf

$$S_y(f) = (r^2/2)\delta(f - \Delta f),$$ (3)

where r is the amplitude coupling coefficient. Inserting this expression for $S_y(f)$ into (2), we obtain for the Allan Deviation

$$\sigma_y(\tau) = r\frac{sin^2(\pi\Delta f\tau)}{\pi\Delta f\tau},$$ (4)

which oscillates with period $1/\Delta f$ as shown in Figure 7. This oscillatory behavior is similar to what we have measured in both of our test configurations. The similarity can be made more evident by adding a white-noise FM contribution to $S_y(f)$ to obtain

$$\sigma_y(\tau) = \left[\frac{10^{-22}}{\tau} + r^2\frac{sin^4(\pi\Delta f\tau)}{(\pi\Delta f\tau)^2}\right]^{1/2}.$$ (5)

This Allan Deviation, plotted in Figure 8, displays a dependence on τ quite similar to what we have observed. The most noticeable difference is that the oscillations in the measured $\sigma_y(\tau)$ are damped out faster than τ^{-1}. This is quite likely due to the fact that Δf, which here was treated as a fixed parameter, is actually a stochastic variable.

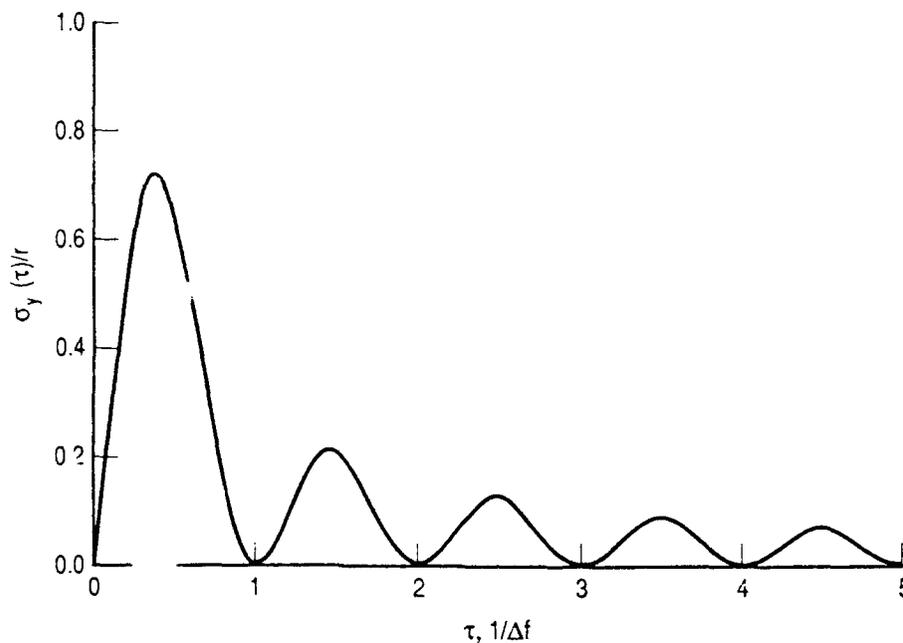
Figure 7. Allan Deviation due to a "bright line" source of fractional frequency fluctuations (normalized by the amplitude coupling coefficient, r) vs. averaging time, in units of reciprocal frequency offset, Δf.
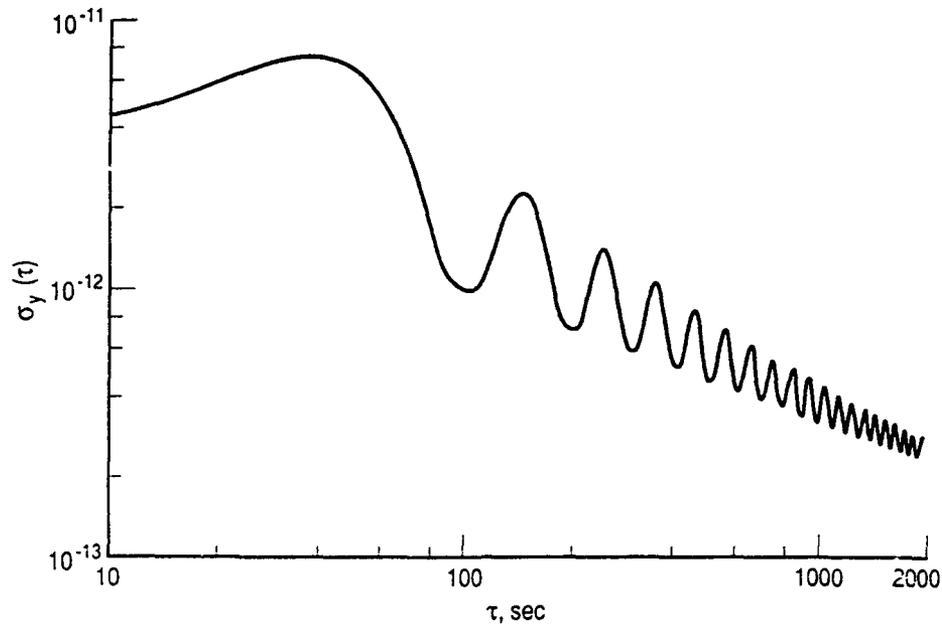
9

Figure 8. Allan Deviation calculated for a spectral density of frequency fluctuations consisting of the sum of a white noise FM term and a "bright line" term.

CONCLUSIONS

This study has shown that the presence of a second, standby atomic frequency standard in a timing system will add an oscillatory term to the system's Allan Variance, thus impairing the system's performance. These oscillations can be fully understood in terms of the linear superposition of the outputs of the two sources, without invoking any clock-dependent mechanism, and, thus, this conclusion has very general validity. The amplitude of these oscillations will depend on the strength of the coupling of the signal from the standby with the signal of the active clock, and can be made negligible by inserting adequate isolation between them. For the configurations we have explored and for the two Efratom RAFS we have used in this study, 70 dB was an adequate level of isolation.

Our study has also shown that under certain circumstances, the output frequency of the active atomic clock may be shifted by coupling the output of the standby clock. This result depends sensitively on the actual hardware and mode of coupling. In the conditions of our study (Efratom RAFS in a worst possible case configuration with the standby clock output connected to the voltage control point of the active clock VCXO), the frequency shift was independent of clock offset and dependent only on the power level being coupled. The coupling coefficient was of the order of $5 \times 10^{-11}/mW$ so that the level of isolation required to reduce the Allan Variance oscillations to acceptable levels (approximately 70 dB) is more than adequate to make this frequency shift negligible.

10

REFERENCE

[1] J. A. Barnes, A. R. Chi, L. S. Cutler, D. J. Healey, D. B. Leeson, T. E. McGunigal, J. A. Mullen. W. L. Smith, R. L. Sydnor, R. F. C. Vessot and G. M. R. Winkler, *Characterization of Frequency Stability*, IEEE Trans. Instr. and Meas., IM-20, 105 (1971).

TECHNOLOGY OPERATIONS

The Aerospace Corporation functions as an "architect-engineer" for national security programs, specializing in advanced military space systems. The Corporation's Technology Operations supports the effective and timely development and operation of national security systems through scientific research and the application of advanced technology. Vital to the success of the Corporation is the technical staff's wide-ranging expertise and its ability to stay abreast of new technological developments and program support issues associated with rapidly evolving space systems. Contributing capabilities are provided by these individual Technology Centers:

Electronics Technology Center: Microelectronics, solid-state device physics, VLSI reliability, compound semiconductors, radiation hardening, data storage technologies, infrared detector devices and testing; electro-optics, quantum electronics, solid-state lasers, optical propagation and communications; cw and pulsed chemical laser development, optical resonators, beam control, atmospheric propagation, and laser effects and countermeasures; atomic frequency standards, applied laser spectroscopy, laser chemistry, laser optoelectronics, phase conjugation and coherent imaging, solar cell physics, battery electrochemistry, battery testing and evaluation.

Mechanics and Materials Technology Center: Evaluation and characterization of new materials: metals, alloys, ceramics, polymers and their composites, and new forms of carbon; development and analysis of thin films and deposition techniques; nondestructive evaluation, component failure analysis and reliability; fracture mechanics and stress corrosion; development and evaluation of hardened components; analysis and evaluation of materials at cryogenic and elevated temperatures; launch vehicle and reentry fluid mechanics, heat transfer and flight dynamics; chemical and electric propulsion; spacecraft structural mechanics, spacecraft survivability and vulnerability assessment; contamination, thermal and structural control; high temperature thermomechanics, gas kinetics and radiation; lubrication and surface phenomena.

Space and Environment Technology Center: Magnetospheric, auroral and cosmic ray physics, wave-particle interactions, magnetospheric plasma waves; atmospheric and ionospheric physics, density and composition of the upper atmosphere, remote sensing using atmospheric radiation; solar physics, infrared astronomy, infrared signature analysis; effects of solar activity, magnetic storms and nuclear explosions on the earth's atmosphere, ionosphere and magnetosphere; effects of electromagnetic and particulate radiations on space systems; space instrumentation; propellant chemistry, chemical dynamics, environmental chemistry, trace detection; atmospheric chemical reactions, atmospheric optics, light scattering, state-specific chemical reactions and radiative signatures of missile plumes, and sensor out-of-field-of-view rejection.